

Electronic Supplementary Information - Bulk properties of aqueous graphene oxide and reduced graphene oxide with surfactants and polymers: adsorption and stability

Thomas M. McCoy,^a Liliana de Campo,^b Anna V. Sokolova,^b
Isabelle Grillo,^c Ekaterina I. Izgorodina,^a Rico F. Tabor^{a,*}

^aSchool of Chemistry, Monash University, Clayton 3800, Australia

^bAustralian Centre for Neutron Scattering, ANSTO, Lucas Heights, New South Wales 2234, Australia

^cInstitut Laue Langevin, F-38042 Grenoble, France

*To whom correspondence should be addressed; E-mail: rico.tabor@monash.edu

This document contains additional figures used for interpretation as well as analysis for the findings presented in the main paper. All fitting parameters used in modelling the SANS/USANS data presented in the main paper are shown as well as explanations for model choice, alternative model considerations and model equations.

Table S1: Mass fractal fitting parameters for graphene oxide (GO) at different concentrations.

GO concentration mg/mL	Scale	Radius	Mass fractal dimension	Cutoff length nm
0.2	1.38×10^{-7}	-	2.85	37.6
1	7.76×10^{-7}	-	2.81	46.3
2	1.40×10^{-6}	-	2.87	41.7
5	3.39×10^{-6}	-	2.85	46.5
10	6.69×10^{-6}	-	2.85	46.2

Aqueous graphene oxide (GO) suspensions were modelled with the mass fractal approximation developed by Mildner and Hall:¹

$$I(q) = scale \times P(q)S(q) + background$$

$$P(q) = F(qR)^2$$

$$F(x) = \frac{3[\sin(x) - x\cos(x)]}{x^3}$$

$$S(q) = \frac{\Gamma(D_m - 1)\zeta^{D_m-1}}{[1 + (q\zeta)^2]^{(D_m-1)/2}} \frac{\sin[(D_m - 1)\tan^{-1}(q\zeta)]}{q}$$

The parameter, R , represents the scattering building blocks for the fractal and D_m is the mass fractal dimension, which must be a value between 0 and 6, and depicts the fractal complexity of the aggregate. The parameter, ζ , is the cut-off length which relates to the overall size of the structures. A more detailed description of the mass fractal model and why it was chosen is discussed in the main paper.

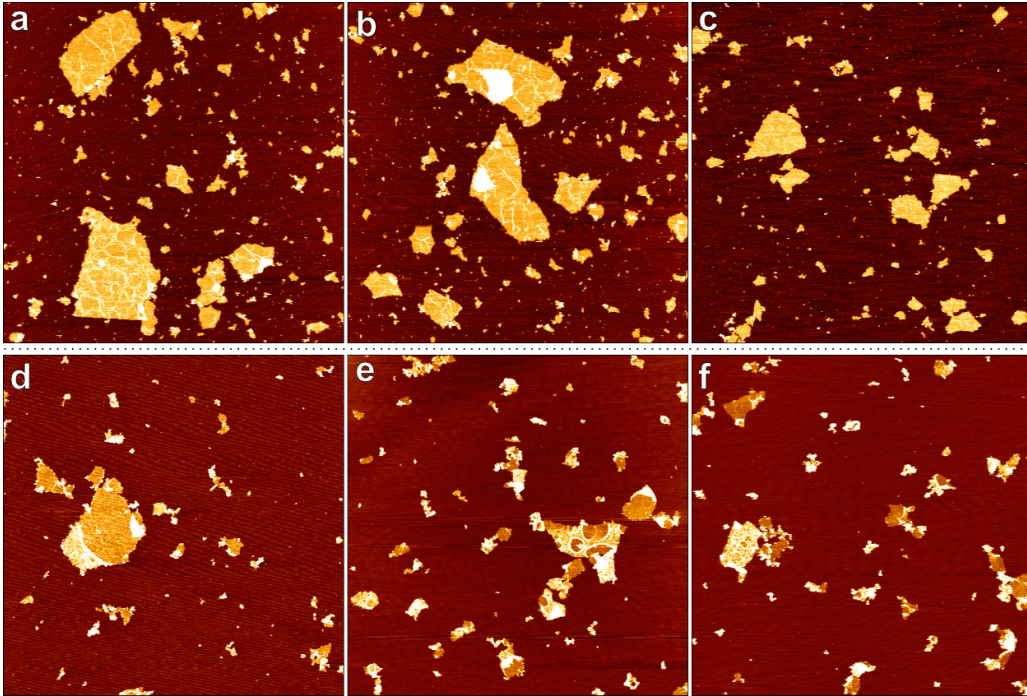


Figure S1: Additional AFM height images of GO (a-c) and rGO (d-f) dried on mica.

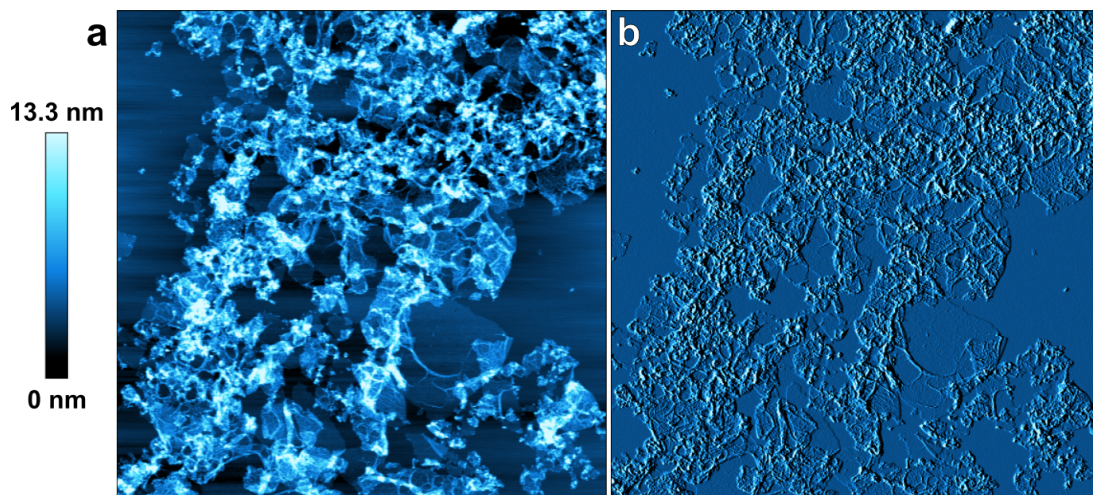


Figure S2: (a) AFM height image of a cluster of rGO dried on mica. (b) The corresponding AFM amplitude image.

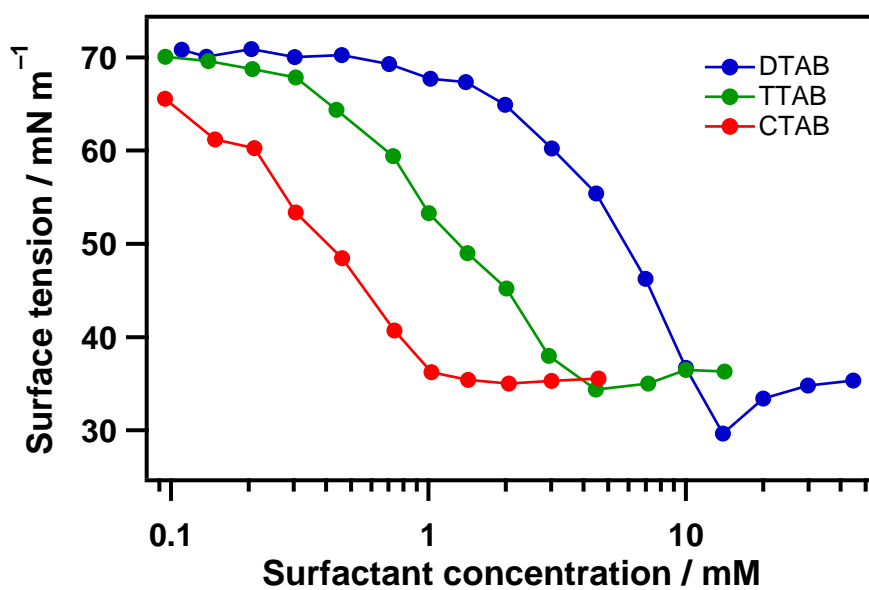


Figure S3: Surface tension data for the cationic surfactants dodecyltrimethylammonium bromide (DTAB), tetradecyltrimethylammonium bromide (TTAB) and cetyltrimethylammonium bromide (CTAB). Measurements were carried out on a custom-made pendant drop apparatus using OpenDrop analysis software.²

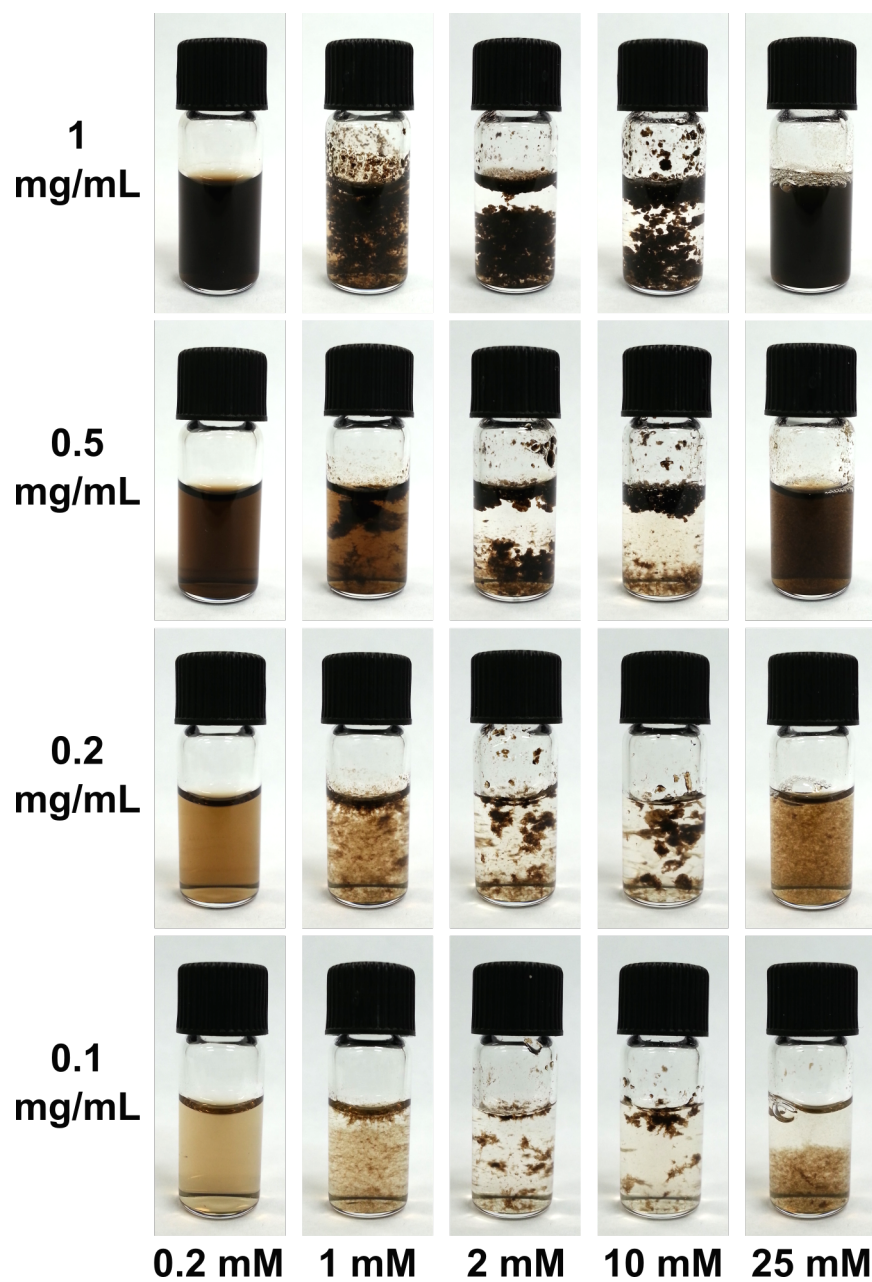


Figure S4: Sample images of GO at various concentrations with the specified concentrations of DTAB added. Used in determining stability phase diagram in main paper.

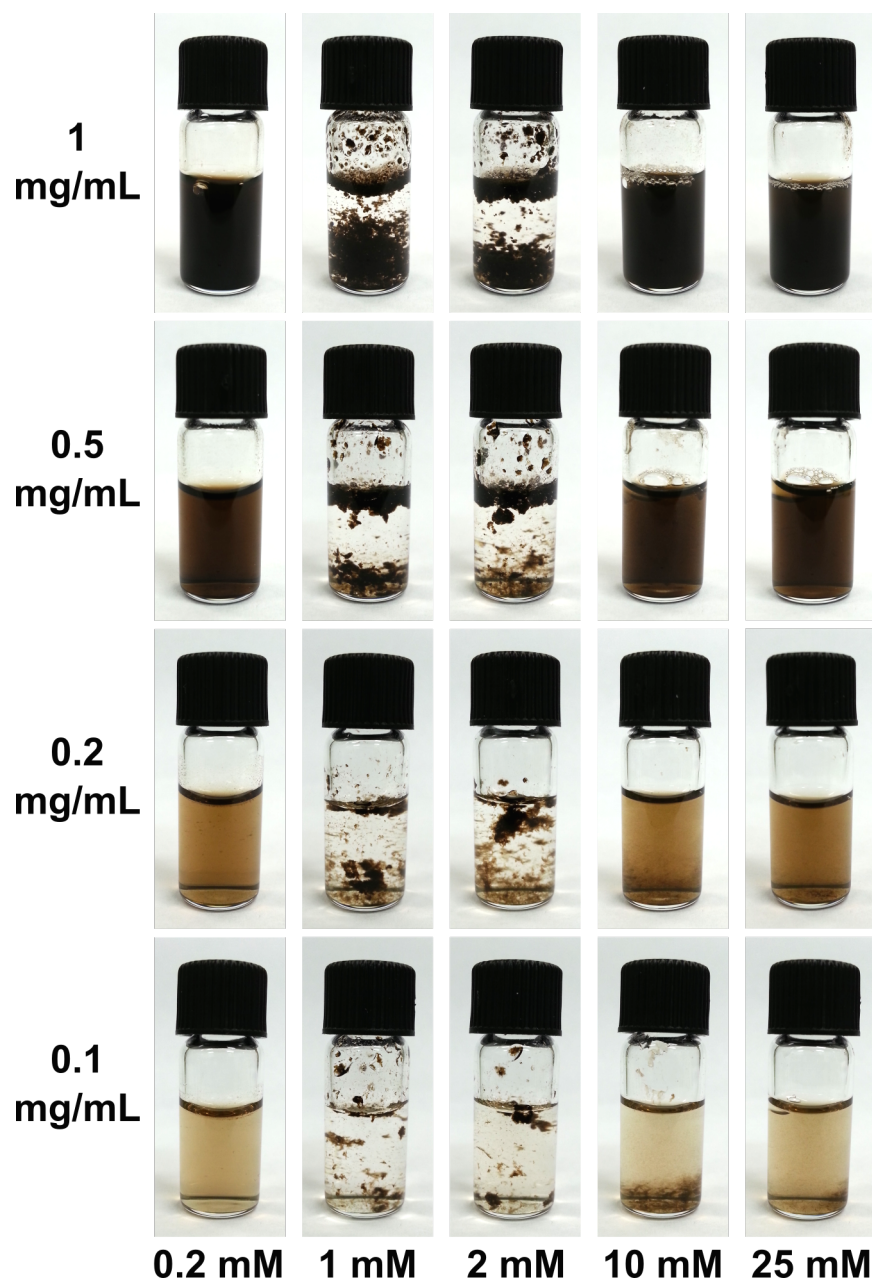


Figure S5: Sample images of GO at various concentrations with the specified concentrations of TTAB added. Used in determining stability phase diagram in main paper.

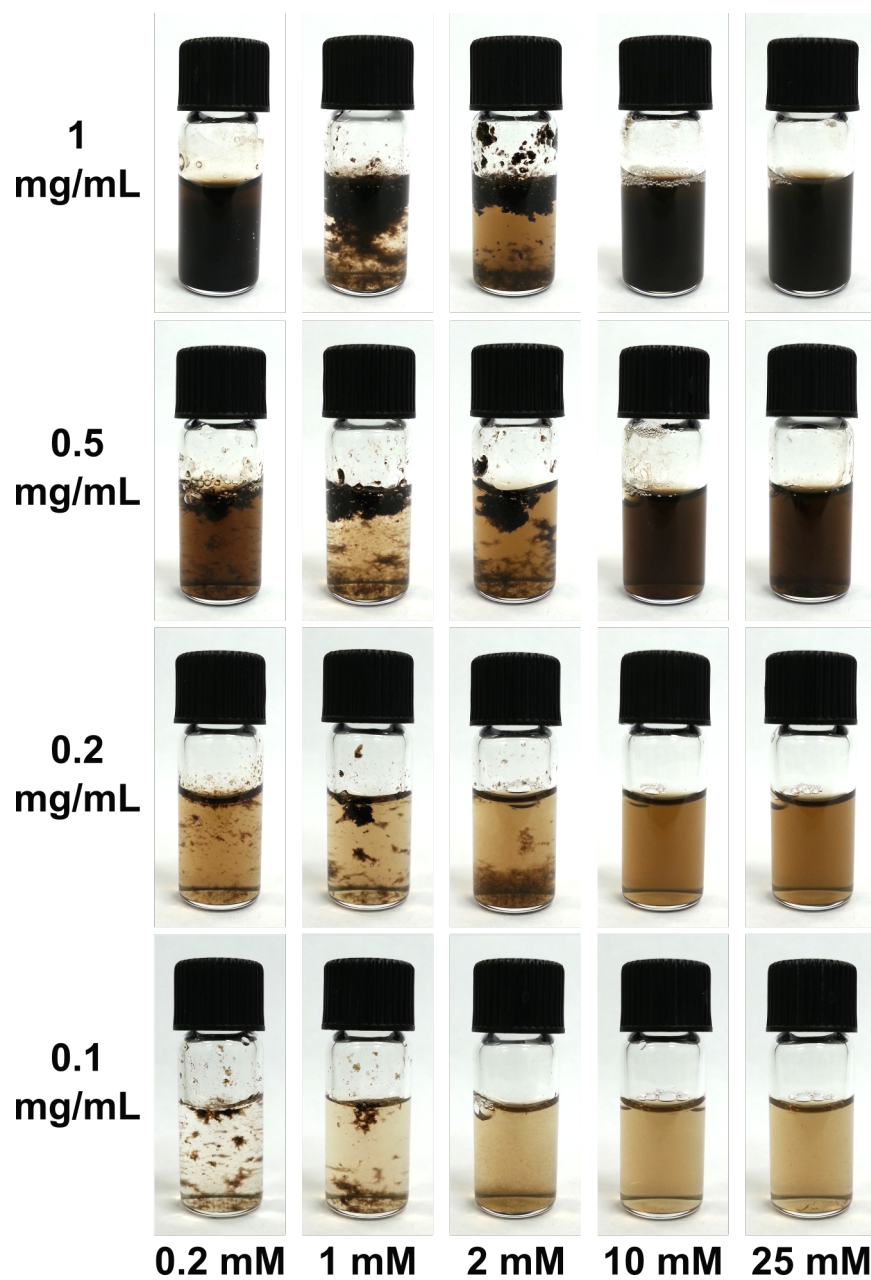


Figure S6: Sample images of GO at various concentrations with the specified concentrations of CTAB added. Used in determining stability phase diagram in main paper.

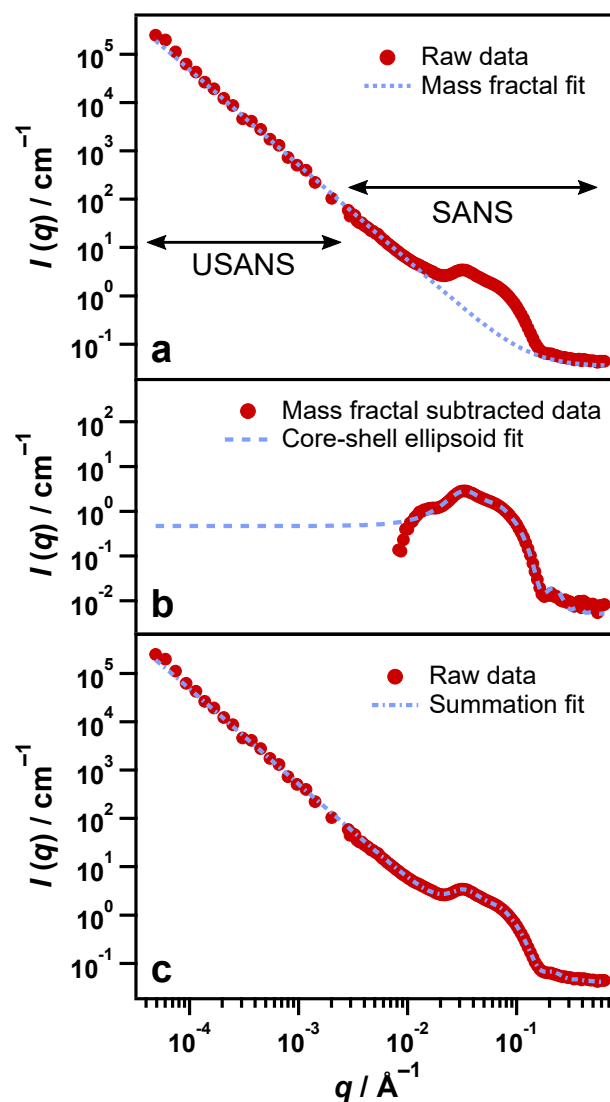


Figure S7: Step-wise process to fitting a summation model to a data set; in this example 25 mM CTAB with 0.1 mg/mL GO: (a) Mass fractal model fit to original SANS/USANS data (low q , fractal region). (b) The mass fractal fit is subtracted from the data and a core-shell ellipsoid model with Hayter-Penfold structure factor is used to fit the new data set (medium q , micelle region). (c) The sum of the mass fractal and ellipsoid models represents the final fit for the original data.

Modelling of systems with cationic and anionic surfactant was done using a core-shell ellipsoid model^{3,4} with inclusion of a Hayter-Penfold structure factor for charged particles.⁵⁻⁹ A core-shell rather than a solid model was used, as in SasView, the core-shell model performed more

accurately in tandem with the structure factor than did the solid ellipsoid model.¹⁰ The core-shell model differs in that there are separate terms for the distances from the micelle core to inner shell boundary, and the inner shell boundary to the outer shell boundary (*i.e.* interface with solvent), each of which have their own respective scattering length densities. The addition of these two lengths would equal the particle radius for the solid ellipsoid model. Note that in all data modelling using the core-shell ellipsoid model, the thickness of the shell was set to 0, hence the model was made to behave the same as the solid ellipsoid model, which is as follows:

$$P(q, \alpha) = \frac{scale}{V} f^2(q) + background$$

where

$$f(q) = \frac{3(\Delta\rho)V \sin[qr(R_a, R_b, \alpha)] - qr \cos[qr(R_a, R_b, \alpha)]}{[qr(R_a, R_b, \alpha)]^3}$$

and

$$r(R_a, R_b, \alpha) = [R_b^2 \sin^2 \alpha + R_a^2 \cos^2 \alpha]^{1/2}$$

The two radii, R_a and R_b , represent the radius along the perpendicular rotational and longitudinal axes of the cylinder ellipsoid respectively. α is the angle between the ellipsoidal axis and the scattering vector q . The Hayter-Penfold structure factor, $S(q)$, is used in conjunction with the ellipsoid form factor and approximates the effects of charge-based interactions between the micelles, where the q vector is defined as:

$$q = \sqrt{q_x^2 + q_y^2}$$

For all cationic systems with structure factor contributions, the summation model method involving the addition of a mass fractal model for the low q region, and the core-shell ellipsoid fit with Hayter-Penfold structure factor for the medium q (micelle) region, to define the overall scattering (Fig. S7). This is because the SasView environment does not have the capacity to simultaneously manage two models as well as a structure factor contribution.

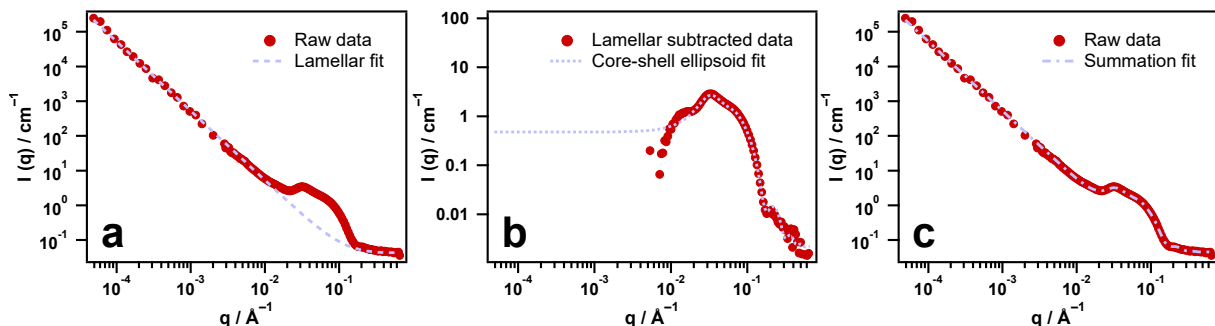


Figure S8: Similar step-wise process as presented for fitting a summation model to the 25 mM CTAB with 0.1 mg/mL GO data set, however in this case we substitute the mass fractal model with a lamellar model. (a) Lamellar model fit to original SANS/USANS data. (b) The lamellar fit is subtracted from the data and a core-shell ellipsoid model with Hayter-Penfold structure factor is used to fit the new data set (medium q , micelle region). (c) The sum of the lamellar and ellipsoid models represents the final fit for the original data.

Because the scattering in the low and ultra-low q region conforms to a slope of q^{-2} , indicating flat surfaces, a lamellar or bilayers model can also be used to define this region (Fig. S8). The lamellar model is from Berghausen.¹¹ The scattering intensity is given by the following equation:

$$I(q) = 2\pi \frac{P(q)}{\delta q^2}$$

where the form factor is given by:

$$P(q) = \frac{2\Delta\rho^2}{q^2} (1 - \cos(q\delta))$$

In both equations, δ is the bilayer thickness in \AA . For all modelling, the scattering length density (\AA^{-2}) of the scatterer and solvent are taken into account and are represented in the equations as ρ , with the difference or 'contrast' being $\Delta\rho$. Unfortunately however, use of the lamellar model does not generate reliable parameters from the modelling of these systems due to the contribution of micelle form and structure factor to the scattering being so prominent. This effect thus masks the true thickness of the aggregates, defined by the point of upturn in the scattering from the background to q^{-2} , meaning the lamellar modelling for low q becomes a balancing exchange between the input scale factor and thickness. Note the error margin for thickness in the provided fit is 2.5 nm, greater than the calculated thickness of 1.1 nm (Table S2). Therefore the lamellar model can not be meaningfully used in systems where a significant

concentration of background micelles are present, and the mass fractal model thus provides a more useful representation of the data.

Table S2: Fitting parameters for the lamellar and core-shell ellipsoid models applied to the 25 mM CTAB with 0.1 mg/mL GO data set (Fig. S8).

Surfactant	Concentration mM	Scale	Bilayer thickness nm	$R_{Eq.}$ nm	$R_{Ax.}$ nm	Volume fraction %	Charge e^{-}	Salt concentration mM
CTAB	25	2.80×10^{-3}	1.1 ± 2.5	2.4	3.7	0.73	49.0	5.24

Table S3: Fitting parameters for cationic surfactants. Aside from pure surfactant solutions, all data are fit using a combination of mass fractal and ellipsoid models with Hayter-Penfold structure factor. $R_{eq.}$ and $R_{ax.}$ are the equatorial and axial radii of the micelles respectively. Scattering length densities of the solvent (D_2O) and micelles were kept constant at 6.3 and $1 \times 10^{-6} \text{ \AA}^{-2}$ respectively.

Carbon nanomaterial	Surfactant	Concentration mM	Scale	Mass fractal dimension	Cutoff length nm	$R_{eq.}$ nm	$R_{ax.}$ nm	Volume fraction %	Charge e^{-}	Salt concentration mM
-	DTAB	25	-	-	-	1.7	2.7	0.34	9.4	5.34
-	TTAB	25	-	-	-	2.0	3.2	0.79	14.6	1.20
-	CTAB	25	-	-	-	2.3	3.8	0.96	21.6	0.12
GO	DTAB	25	4.45×10^{-4}	1.87	1500	1.9	1.5	0.43	7.2	0.02
GO	TTAB	25	8.38×10^{-4}	1.77	2000	2.1	2.8	0.60	24.1	1.43
GO	CTAB	25	5.95×10^{-4}	1.98	100000	2.4	3.6	0.72	49.1	4.83
rGO	DTAB	25	4.00×10^{-4}	1.71	4000	2.2	1.2	0.44	10.8	1.37
rGO	TTAB	25	4.84×10^{-4}	1.76	3000	2.1	2.8	0.64	18.1	0.12
rGO	CTAB	25	6.04×10^{-4}	1.79	5652.2	2.4	3.4	0.80	25.9	0.17

Table S4: Fitting parameters for 2.5 mM CTAB samples. Aside from blank 2.5 mM CTAB, all data are fit using a sum of mass fractal and ellipsoid models. At this surfactant concentration, no structure factor was required. $R_{eq.}$ and $R_{ax.}$ are the equatorial and axial radii of the micelles respectively. Scattering length densities of the solvent (D_2O) and micelles were kept constant at 6.3 and $1 \times 10^{-6} \text{ \AA}^{-2}$ respectively.

Carbon nanomaterial	Surfactant	Concentration mM	Scale 1	Particle radius nm	Mass fractal dimension	Cutoff length nm	Scale 2	$R_{Eq.}$ nm	$R_{Ax.}$ nm
-	CTAB	2.5	-	-	-	-	1.09×10^{-3}	3.1	1.8
GO	CTAB	2.5	2.74×10^{-4}	5.1	2.14	39.1	1.11×10^{-3}	2.7	1.0
rGO	CTAB	2.5	1.66×10^{-4}	4.8	2.07	63.7	1.03×10^{-3}	3.0	1.4

Table S5: Ellipsoid model fitting parameters with Hayter-Penfold structure factor for anionic surfactants. $R_{eq.}$ and $R_{ax.}$ are the equatorial and axial radii of the micelles respectively. Scattering length densities of the solvent (D_2O) and micelles were kept constant at 6.3 and $1 \times 10^{-6} \text{ \AA}^{-2}$ respectively.

Carbon Nanomaterial	Surfactant	Concentration mM	$R_{eq.}$ nm	$R_{ax.}$ nm	Volume fraction %	Charge e^-	Salt concentration mM
-	SDS	25	1.8	2.7	0.52	12.6	1.16
-	AOT	25	1.2	2.6	0.81	14.9	1.86
GO	SDS	25	1.7	2.6	0.48	12.2	1.35
GO	AOT	25	1.2	2.5	0.73	19.7	6.15
rGO	SDS	25	1.7	2.7	0.49	17.4	1.98
rGO	AOT	25	1.2	2.5	0.72	20.0	6.56

Table S6: Fitting parameters for Triton X-100. Aside from the pure surfactant samples, all data are fit using a sum of mass fractal and cylinder models. $R_{eq.}$ and $R_{ax.}$ are the equatorial and axial radii of the micelles respectively. Scattering length densities of the solvent (D_2O) and micelles were kept constant at 6.3 and $1 \times 10^{-6} \text{ \AA}^{-2}$ respectively.

Carbon nanomaterial	Surfactant	Concentration mM	Scale 1	Particle radius nm	Mass fractal dimension	Cutoff length nm	Scale 2	Radius nm	Length nm
-	Triton X-100	10	-	-	-	-	6.23×10^{-3}	2.1	8.8
GO	Triton X-100	10	6.93×10^{-4}	-	1.68	20000.0	4.59×10^{-3}	2.2	7.4
rGO	Triton X-100	10	5.30×10^{-4}	1.0	1.70	100.0	4.80×10^{-3}	2.3	7.4
-	Triton X-100	1	-	-	-	-	4.06×10^{-4}	2.3	7.4
GO	Triton X-100	1	8.32×10^{-5}	7.0	2.03	50.0	4.23×10^{-4}	2.7	2.8
rGO	Triton X-100	1	6.53×10^{-5}	4.8	2.11	53.7	1.94×10^{-3}	2.8	0.5

The rod/cylinder (or ellipsoid) model used in modelling data with TX-100 was from Feigin and Svergun,¹⁰ follows the same principles as the ellipsoid model and is explained in detail above.

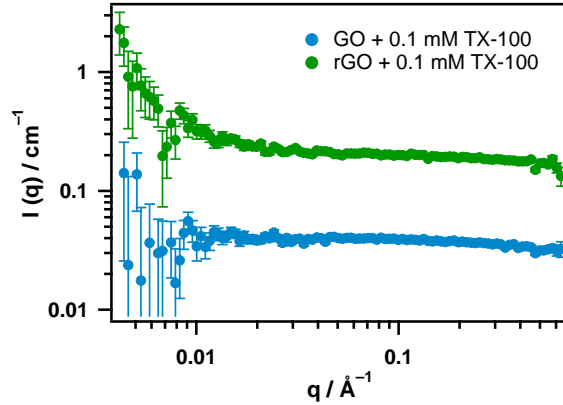


Figure S9: SANS data for 0.1 mg/mL GO and rGO with 0.1 mM Triton X-100. The data for rGO has been offset for clarity.

Table S7: Fitting parameters for $C_{12}E_6$ with GO and rGO. These data were fit using cylinder models for the pure surfactant samples, and a sum of mass fractal and cylinder models where carbon nanomaterials and surfactants were present. Scattering length densities of the solvent (D_2O) and micelles were kept constant at 6.3 and $1 \times 10^{-6} \text{ \AA}^{-2}$ respectively.

Carbon nanomaterial	Surfactant	Concentration mM	Scale 1	Particle radius nm	Mass fractal dimension	Cutoff length nm	Scale 2	Radius nm	Length nm
-	$C_{12}E_6$	10	-	-	-	-	5.61×10^{-3}	2.1	10.6
GO	$C_{12}E_6$	10	1.19×10^{-3}	1.5	1.73	1000.0	4.94×10^{-3}	3.0	3.2
rGO	$C_{12}E_6$	10	5.05×10^{-5}	1.7	1.98	9845.0	6.27×10^{-3}	2.0	8.9
-	$C_{12}E_6$	1	-	-	-	-	6.51×10^{-4}	1.8	8.5
rGO	$C_{12}E_6$	1	4.15×10^{-5}	-	1.99	2118	5.33×10^{-4}	1.6	9.2

Table S8: Fitting parameters for 1 mM $C_{12}E_6$ with GO. This data set was fit using a sum of lamellar and cylinder models. Scattering length densities of the solvent (D_2O) and micelles were kept constant at 6.3 and $1 \times 10^{-6} \text{ \AA}^{-2}$ respectively.

Carbon nanomaterial	Surfactant	Concentration mM	Scale 1	Radius nm	Length nm	Scale 2	Thickness nm
GO	$C_{12}E_6$	1	7.02×10^{-3}	0.4	3.5	1.59×10^{-4}	9.6

Table S9: Flexible cylinder fitting parameters for pure C₁₂E₅ samples. At 10 mM, a two-power law model was also used to fit the USANS region. Scattering length densities of the solvent (D₂O) and micelles were kept constant at 6.3 and $1 \times 10^{-6} \text{ \AA}^{-2}$ respectively.

Surfactant	Concentration mM	Scale 1	Lower q power	Higher q power	Crossover point \AA^{-1}	Scale 2	Radius nm	Length nm	Kuhn length nm
C ₁₂ E ₅	10	5.48×10^{-4}	1.64	0.41	6.30×10^{-4}	5.47×10^{-3}	2.1	207.9	26.9
C ₁₂ E ₅	1	-	-	-	-	5.12×10^{-4}	1.8	103.3	11.7

The flexible cylinder or 'worm' model is presented in Pederson *et al.*:¹²

$$I_{WC}(q, L, b, R_{CS}) = c \Delta \rho_m^2 M S_{WC}(q, L, b) P_{CS}(q, R_{CS})$$

Where c is the surfactant concentration, M is the molecular weight of the micelles and $S_{WC}(q, L, b)$ represents the scattering function of a semi-flexible chain without volume effects in which L/b is the number of statistical segments in the chain:

$$S_{WC}(q, L, b) = [(1 - \chi(q, L, b)) S_{chain}(q, L, b) + \chi(q, L, b) S_{rod}(q, L)] \Gamma(q, L, b)$$

Chen *et al* included corrections to the formula by accounting for intermicellar interactions by including the parameter in the following equation,¹³ which is currently used in modelling flexible cylinders in SasView:

$$f_{corr}(q) w(qR_G) [1.22(qR_G)^{-1/0.585} + 0.4288(qR_G)^{-2/0.585} - 1.651(qR_G)^{-3/0.585}]$$

Table S10: Fitting parameters for C₁₂E₅ with GO and rGO. Data were fit using a sum of mass fractal and flexible cylinder models. Scattering length densities of the solvent (D₂O) and micelles were kept constant at 6.3 and $1 \times 10^{-6} \text{ \AA}^{-2}$ respectively.

Carbon nanomaterial	Surfactant	Concentration mM	Scale 1	Particle radius nm	Mass fractal dimension	Cutoff length nm	Scale 2	Radius nm	Length nm	Kuhn length nm
GO	C ₁₂ E ₅	10	7.21×10^{-4}	-	1.88	2217.2	4.01×10^{-3}	2.1	269.1	20.5
rGO	C ₁₂ E ₅	10	6.50×10^{-5}	-	2.12	6000.0	5.22×10^{-3}	2.1	165.4	28.6
rGO	C ₁₂ E ₅	1	4.64×10^{-4}	-	1.64	625.5	1.63×10^{-5}	3.9	100.0	6.8

Table S11: Fitting parameters for 1 mM $C_{12}E_5$ with GO. This data set was fit using a sum of lamellar and flexible cylinder models. Scattering length densities of the solvent (D_2O) and micelles were kept constant at 6.3 and $1 \times 10^{-6} \text{ \AA}^{-2}$ respectively.

Carbon nanomaterial	Surfactant	Concentration mM	Scale 1	Radius nm	Length nm	Scale 2	Thickness nm
GO	$C_{12}E_5$	1	2.61×10^{-3}	0.8	1.5	2.18×10^{-4}	9.8

Table S12: Fitting parameters for $C_{12}E_4$ with GO and rGO. All data including pure surfactant samples were fit using a sum of mass fractal and vesicle models. Scattering length densities of the solvent (D_2O) and micelles were kept constant at 6.3 and $1 \times 10^{-6} \text{ \AA}^{-2}$ respectively.

Carbon nanomaterial	Surfactant	Concentration mM	Scale 1	Particle radius nm	Mass fractal dimension	Cutoff length nm	Volume fraction %	Radius nm	Polydispersity of radius %	Thickness nm
-	$C_{12}E_4$	10	1.83×10^{-3}	1.6	2.02	466.1	0.12	25.1	36.5	4.8
GO	$C_{12}E_4$	10	1.39×10^{-3}	2.7	2.12	832.9	0.38	30.8	47.2	1.4
rGO	$C_{12}E_4$	10	5.45×10^{-4}	-	2.16	719.9	0.31	33.0	22.4	3.5
-	$C_{12}E_4$	1	4.41×10^{-6}	-	2.41	2948.6	0.04	38.3	27.8	3.8
GO	$C_{12}E_4$	1	3.51×10^{-4}	8.3	2.10	1281.6	0.07	4.1	10.4	0.4
rGO	$C_{12}E_4$	1	4.35×10^{-5}	4.2	2.36	3892.2	0.11	15.5	47.1	0.6

The model providing the form factor, $P(q)$, for a unilamellar vesicle is from Guinier and Fournet,¹⁴ and is represented by the following:

$$P(q) = \frac{scale}{V_{shell}} \left[\frac{3V_1(\rho_1 - \rho_2)J_1(qR_1)}{(qR)_1} + \frac{3V_2(\rho_2 - \rho_{solv})J_1(qR_2)}{(qR)_2} \right]^2 + background$$

Where V_{shell} is the volume of the shell, V_1 is the volume of the core and V_2 is the total volume. R_1 is the radius of the core and R_1 is the radius from the core to the shell in \AA . $J_1 = (\sin x - x \cos x)/x^2$. Polydispersity for vesicle radius was also included in the fitting algorithm for $C_{12}E_4$ systems.

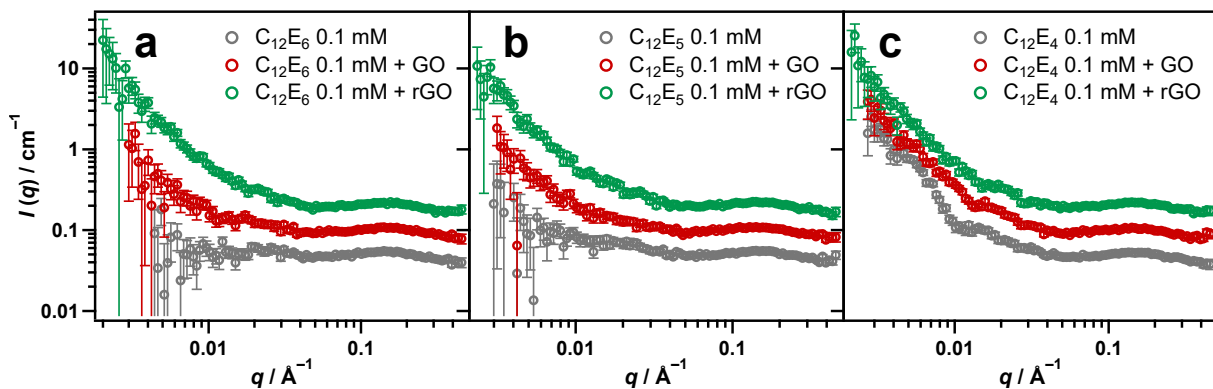


Figure S10: SANS data for 0.1 mM $C_{12}E_6$ (a), 0.1 mM $C_{12}E_5$ (b) and 0.1 mM $C_{12}E_4$ (c) with 0.1 mg/mL GO and rGO. The data for GO and rGO has been offset by multiplication for clarity.

Table S13: Fitting parameters for erucyl amidopropyl betaine (EAPB) and oleyl amidopropyl betaine (OAPB). Aside from the pure surfactant samples, all data are fit using a sum of mass fractal and flexible cylinder models. Radius is the cross-sectional radius of the wormlike micelles and Kuhn length is the apparent length over which the wormlike structures appear rigid. Scattering length densities of the solvent (D_2O) and micelles were kept constant at 6.3 and $1 \times 10^{-6} \text{ \AA}^{-2}$ respectively.

Carbon nanomaterial	Surfactant	Concentration mM	Scale 1	Particle radius nm	Mass fractal dimension	Cutoff length nm	Scale 2	Radius nm	Kuhn length nm	Length nm
-	OAPB	10	-	-	-	-	5.00×10^{-3}	2.2	74.6	126.3
-	EAPB	10	-	-	-	-	9.43×10^{-3}	2.9	38.5	34.9
GO	OAPB	10	9.52×10^{-4}	2.6	2.0	1341.4	3.24×10^{-3}	1.9	59.8	847.3
rGO	OAPB	10	3.02×10^{-4}	1.0	2.0	500.0	3.58×10^{-3}	2.2	29.3	4,626.1
GO	EAPB	10	1.37×10^{-3}	2.0	2.0	4264.8	1.54×10^{-3}	2.8	15.6	10000.0
rGO	EAPB	10	8.17×10^{-4}	1.8	2.0	44.6	3.22×10^{-3}	2.9	61.3	245.0
-	OAPB	1	-	-	-	-	4.02×10^{-4}	2.4	54.6	218.6
GO	OAPB	1	1.82×10^{-4}	6.5	2.0	79.0	4.82×10^{-4}	1.4	34.0	136.0
rGO	OAPB	1	2.15×10^{-4}	6.6	2.0	200.0	6.74×10^{-4}	0.9	39.2	100.3
GO	OAPB	0.1	-	-	-	-	-	-	-	-
GO	EAPB	0.1	7.47×10^{-6}	-	2.4	35.8	-	-	-	-

Modelling for samples with EAPB and OAPB was carried out using the same flexible cylinder model as for $C_{12}E_5$.

Table S14: First level unified power model fitting parameters for polyethylene glycol (PEG) and Pluronic F127 polymer samples. R_g is the radius of gyration of the aggregates while power, B_i and G_i are parameters of the Debye equation.

Carbon Nanomaterial	Polymer	Concentration mg/mL	R_g nm	Power	B_i cm ⁻¹	G_i cm ⁻¹
-	PEG	1.5	22.2	1.80	0.008	59.5
-	Pluronic F127	1.5	4.0	0.10	1.787	2.7
GO	PEG	1.5	15.2	1.37	0.007	8.1
GO	Pluronic F127	1.5	10.7	1.34	0.032	8.0
rGO	PEG	1.5	36.3	1.54	0.036	547.1
rGO	Pluronic F127	1.5	26.7	1.20	0.094	124.2

For polymer and GO/rGO systems, a unified power model was employed to approximate the scattering of the mass fractal clusters (*i.e.* the GO and rGO sheets) and random coils (*i.e.* the polymers) *in situ*.^{15,16} This model uses multiple exponential or power laws (referred to as levels) to define the scattering of a variety of particle types and is ideal for mass fractal systems. The function for calculating scattering intensity is:

$$I(q) = background + \sum_{i=1}^N \left[G_i \exp\left(-\frac{q^2 R_{gi}^2}{3}\right) + B_i \exp\left(-\frac{q^2 R_{g(i+1)}^2}{3}\right) \left(\frac{1}{q_i^*}\right)^{P_i} \right]$$

where

$$q_i^* = q \left[erf\left(\frac{q R_{gi}}{\sqrt{6}}\right) \right]^{-3}$$

Each level is represented by one of the following parameters: G_i , R_{gi} , B_i and P_i .

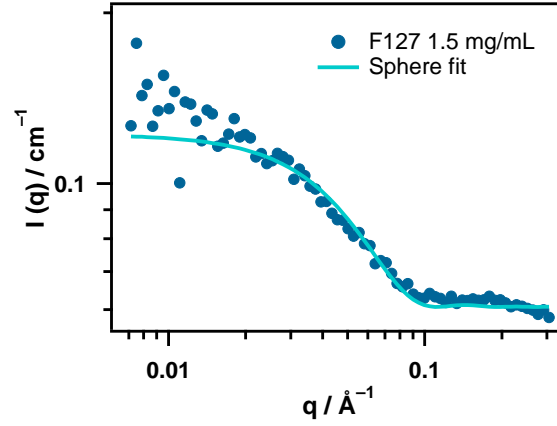


Figure S11: SANS data for pure 1.5 mg/mL Pluronic F127 modelled using a spheres model instead of a unified power model.

Table S15: Sphere model fitting parameters for pure Pluronic F127 polymer. Scattering length densities of the solvent (D_2O) and micelles were kept constant at 6.3 and $1 \times 10^{-6} \text{ \AA}^{-2}$ respectively.

Carbon Nanomaterial	Polymer	Concentration mg/mL	Radius nm
-	Pluronic F127	1.5	4.0

Details for the sphere model used to fit 1.5 mg/mL Pluronic F127 is from Guinier and Fournet.¹⁴ The equation for the scattering intensity, $I(q)$, as a function of the scattering vector, q , for spheres is as follows:

$$I(q) = \frac{scale}{V} \left[\frac{3V(\Delta\rho)(\sin(qr) - qr \cos(qr))}{(qr)^3} \right]^2 + background$$

Where V is the volume of the scatterer, r is the radius of the sphere in \AA , $scale$ is the volume fraction, $\Delta\rho$ is the contrast (difference in scattering length density between the solvent and scatterer) and the background is in cm^{-1} .

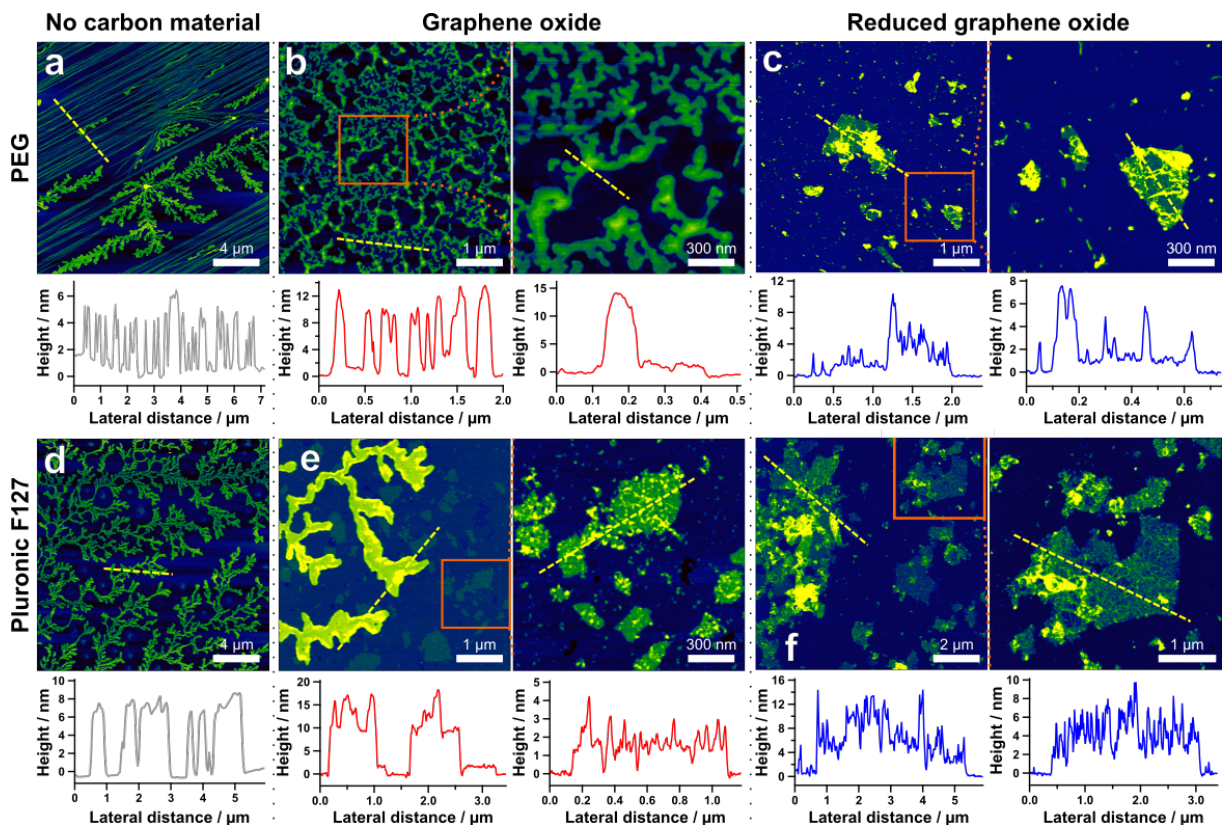


Figure S12: AFM images of 0.1 mg/mL of polymer with or without 0.1 mg/mL GO or rGO dispersions: (a) AFM height images of PEG (a) with GO (b) and rGO (c). AFM height images of pluronic F127 (d) with GO (e) and rGO (f). Height profiles corresponding to the dashed yellow cross sections are shown below each respective image. Higher magnification images correspond to the area inside the orange boxes. Samples are dried on mica substrate.

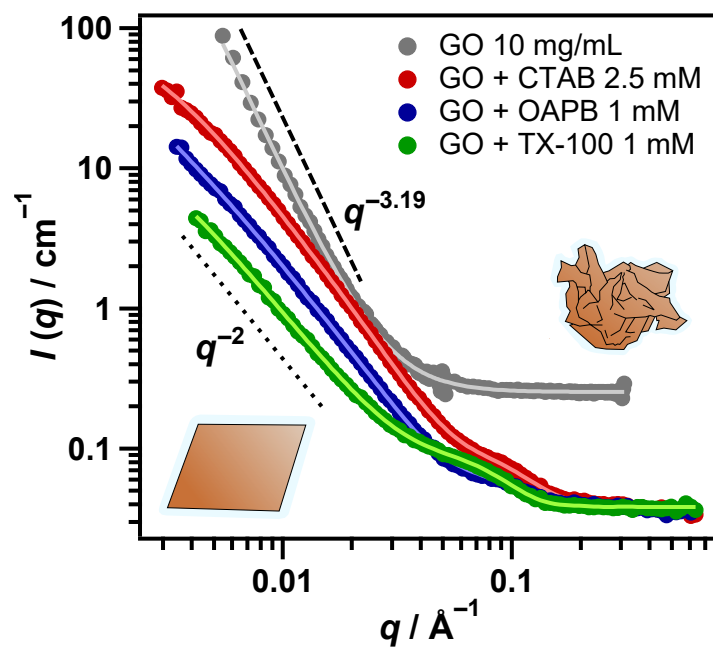


Figure S13: SANS data demonstrating the change in slope from q^{-3} (crumpled fractal sheets) for pure aqueous GO dispersion at 10 mg/mL to q^{-2} (flat surfaces) with the inclusion of either a cationic (CTAB), zwitterionic (OAPB) or nonionic (TX-100) surfactant. Concentration of GO in samples with surfactant is 0.1 mg/mL. The data set with 10 mg/mL GO has been offset by multiplication ($\times 5$) for clarity.

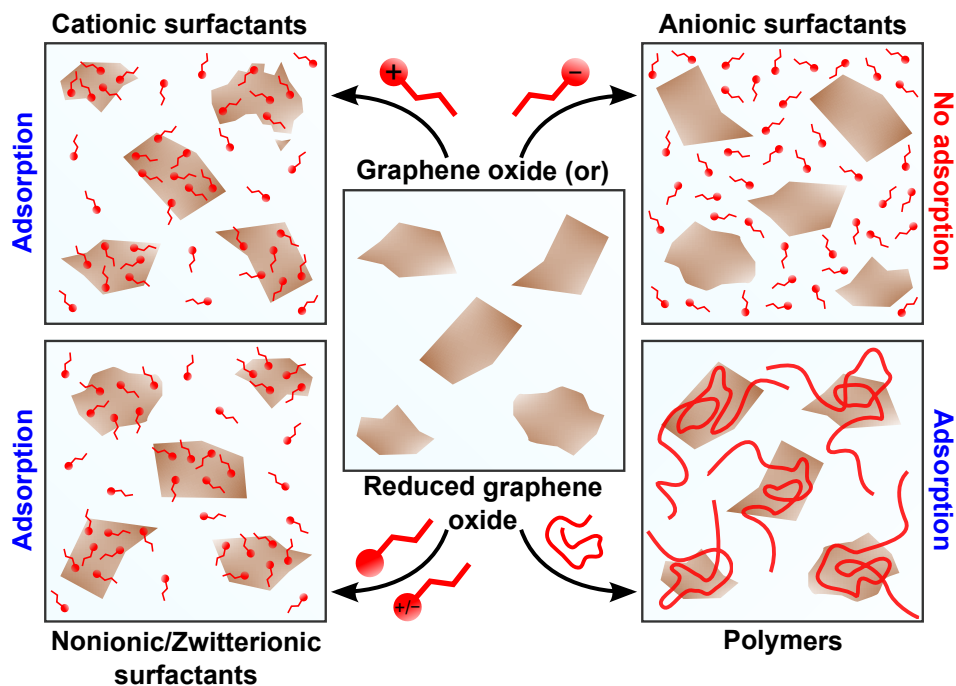


Figure S14: Schematic summarising adsorption interactions of graphene oxide and reduced graphene oxide with each surfactant class and polymers investigated in this study.

References

- [1] Mildner, D. F. R., Hall, P. L. Small-angle scattering from porous solids with fractal geometry. *J. Phys. D: Appl. Phys.* **1986** *19*, 1535–1545.
- [2] Berry, J. D., Neeson, M. J., Dagastine, R. R., Chan, D. Y., Tabor, R. F. Measurement of Surface and Interfacial Tension using Pendant Drop Tensiometry. *J. Colloid Interface Sci.* **2015** *454*, 226 – 237.
- [3] Kotlarchyk, M., Chen, S.-H. Analysis of small angle neutron scattering spectra from polydisperse interacting colloids. *J. Chem. Phys.* **1983** *79*, 2461–2469.
- [4] Berr, S. Solvent isotope effects on alkytrimethylammonium bromide micelles as a function of alkyl chain length. *J. Phys. Chem.* **1987** *91*, 4760–4765.
- [5] Hayter, J. B., Penfold, J. An analytic structure factor for macroion solutions. *Mol. Phys.* **1981** *42*, 109–118.

- [6] Hayter, J. B., Penfold, J. Self-consistent Structural and Dynamic Study of Concentrated Micelle Solutions. *J. Chem. Soc., Faraday Trans. I* **1981** *77*, 1851–1863.
- [7] Hansen, J.-P., Hayter, J. B. A rescaled MSA structure factor for dilute charged colloidal dispersions. *Molecular Physics* **1982** *46*, 651–656.
- [8] Hayter, J. B., Penfold, J. Determination of Micelle Structure and Charge by Small-Angle Neutron Scattering. *Colloid Polym. Sci.* **1983** *261*, 1022–1030.
- [9] Wu, C., Chan, D. Y., Tabor, R. F. A simple and accurate method for calculation of the structure factor of interacting charged spheres. *J. Colloid Interface Sci.* **2014** *426*, 80–82.
- [10] Feigin, L., Svergun, D. I., Taylor, G. W. General principles of small-angle diffraction. In *Structure analysis by small-angle X-ray and neutron scattering*. Springer, **1987**, pages 25–55.
- [11] Berghausen, J., Zipfel, J., Lindner, P., Richtering, W. Influence of water-soluble polymers on the shear-induced structure formation in lyotropic lamellar phases. *J. Phys. Chem. B* **2001** *105*, 11081–11088.
- [12] Pedersen, J. S., Schurtenberger, P. Scattering Functions of Semiflexible Polymers with and without Excluded Volume Effects. *Macromolecules* **1996** *29*, 7602–7612.
- [13] Chen, W.-R., Butler, P. D., Magid, L. J. Incorporating intermicellar interactions in the fitting of SANS data from cationic wormlike micelles. *Langmuir* **2006** *22*, 6539–6548.
- [14] Guinier, A., Fournet, G., Walker, C. Small angle scattering of X-rays. *J. Wiley & Sons, New York* **1955** .
- [15] Beaucage, G. Approximations leading to a unified exponential/power-law approach to small-angle scattering. *J. Appl. Crystallogr.* **1995** *28*, 717–728.
- [16] Beaucage, G. Small-angle scattering from polymeric mass fractals of arbitrary mass-fractal dimension. *J. Appl. Crystallogr.* **1996** *29*, 134–146.